Thin Film Analysis by X-Ray Scattering

Mario Birkholz

With Contributions by

Paul F. Fewster
Christoph Genzel

WILEY-VCH Verlag GmbH & Co. KGaA

Mario Birkholz
Thin Film Analysis by X-Ray Scattering

Related Titles

Messerschmidt, A.

A Practical Guide to X-Ray Crystallography of Biomacromolecules

Principles and Applications

approx. 350 pages with 8 figures
Hardcover
ISBN 3-527-31396-6

Talman, R.

Electron Accelerators as X-Ray Sources

Especially the Energy Recovery Linac

approx. 470 pages with approx. 150 figures and approx. 25 tables
Hardcover
ISBN 3-527-40590-9

Tsuji, K., Injuk, J., Van Grieken, R. (eds.)

X-Ray Spectrometry

Recent Technological Advances

616 pages
2003
Hardcover
ISBN 0-471-48640-X

Bubert, H., Jenett, H. (eds.)

Surface and Thin Film Analysis

A Compendium of Principles, Instrumentation, and Applications

353 pages with 200 figures and 8 tables
2002
Hardcover
ISBN 3-527-30458-4

Janssens, K. H. A., Adams, F. C. V., Rindby, A. (eds.)

Microscopic X-Ray Fluorescence Analysis

433 pages
2000
Hardcover
ISBN 0-471-97426-9

Lifshin, E. (ed.)

X-ray Characterization of Materials

277 pages with 142 figures and 19 tables
1999
Hardcover
ISBN 3-527-29657-3

Thin Film Analysis by X-Ray Scattering

Mario Birkholz

With Contributions by

Paul F. Fewster
Christoph Genzel

WILEY-VCH Verlag GmbH & Co. KGaA

The Author(s) of this Book

Dr. Mario Birkholz
IHP Microelectronics GmbH
Im Technologiepark 25
15236 Frankfurt (Oder)
Germany
E-mail: birkholz@ihp-microelectronics.com

Thin Film Analysis and Technology
www.thinfilm-at.com

With Contributions by

Prof. Paul F. Fewster
PANalytical Research Centre
Sussex Innovation Centre
Science Park Square
Falmer, Brighton
BN1 9SB
UK
E-mail: Paul.Fewster@PANalytical.com

PD Dr. rer. nat. Christoph Genzel
Hahn-Meitner-Institut Berlin
Bereich Strukturforschung
c/o BESSY
Albert-Einstein-Straße 15
12489 Berlin
Germany
E-mail: genzel@hmi.de

Cover
G. Schulz, Fußgönheim

Library of Congress Card No.: applied for
British Library Cataloging-in-Publication Data:
A catalogue record for this book is available from the British Library.
Bibliographic information published by Die Deutsche Bibliothek
Die Deutsche Bibliothek lists this publication in the Deutsche Nationalbibliografie; detailed bibliographic data is available in the Internet at http://dnb.ddb.de.

Typesetting TypoDesign Hecker GmbH, Leimen
Printing betz-druck GmbH, Darmstadt
Binding J. Schäffer GmbH i. G., Grünstadt

Printed in the Federal Republic of Germany
Printed on acid-free paper

ISBN-13: 978-3-527-31052-4
ISBN-10: 3-527-31052-5

Table of Contents

Preface

Mario Birkholz

Thin films have become an important branch of materials science and technology over the last few decades. A thin film is considered in this book as having a thickness between about 1 nm and some 10 µm. Their first application was probably in the field of decorative coatings, but in the last century many other applications in microelectronics, optics, data storage, sensorics, protection and other purposes have had a large impact on the development of thin films and related deposition techniques. Figure 1 displays a variety of thin-film applications from the areas mentioned. Depending on the intended application, thin films are made of metals, inorganic compounds, organic compounds or from biological molecules. The task of the thin-film developer is easily described by stating that the deposition process has to be optimized such that the arrangement of atoms enables the film to fulfill the intended functionality.

Since structure and function are intimately related properties in any material, the characterization of structural properties is a very relevant issue in thin-film development. This book is concerned with the structural analysis of thin films by x-ray scattering procedures. There exist various other characterization techniques like electron microscopy, scanning tunneling methods, ion beam scattering, magnetic resonance, optical spectroscopy and others by which important structure properties may be elucidated. Here, however, the focus is on x-ray scattering. The suitability of this technique for thin-film analysis is mainly motivated by two reasons:

1. The wavelengths of x-rays are of the order of atomic distances in condensed matter, which especially qualifies their use as structural probes.
2. X-ray scattering techniques are nondestructive and leave the investigated sample or – more importantly – the produced device intact.

Electron microscopy might be considered of comparative importance for the characterization of structure and morphology. This technique is a complementary one to x-ray scattering, since it probes a rather confined volume of the sample, whereas x-ray scattering yields information from a much larger volume. Therefore, some micrographs from electron microscopy will appear in the text, but the reader is referred to the special literature for an introduction to the subject.

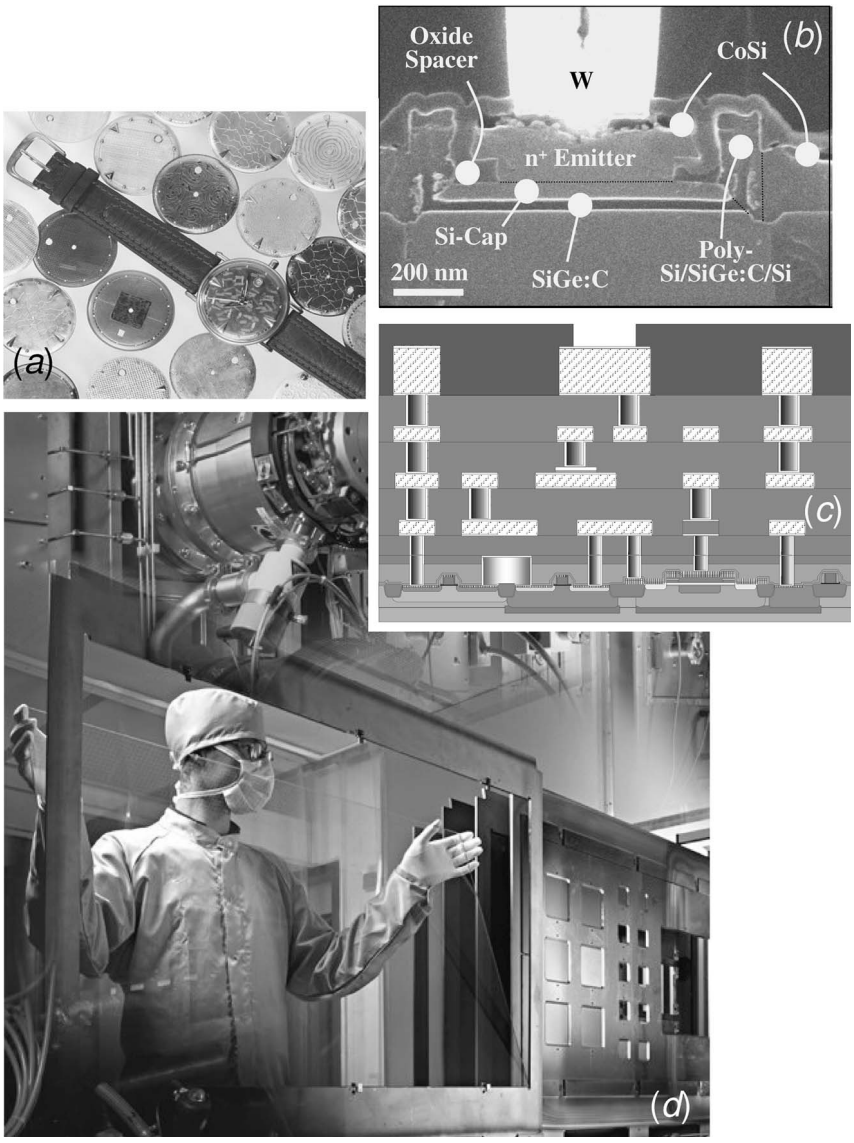

Various examples from thin film applications: (a) decorative coatings on metal dials, (b) scanning electron micrograph of cross-section from SiGe:C heterojunction bipolar transistor, (c) schematic of SiGe:C BiCMOS architecture with four metal layers, (d) processing of window glass for optical coating (Fotograf: Rainer Maier, BFF, Wittmar), (e) identity card with optical data storage made from bacterial purple membrane containing the protein bacteriorhodopsin and example of stored pixel patterns, (f) cemented carbide cutting insert with c-BN protective coating and (g) tip of a diamond-coated abrasive pencil of 60 µm diameter (figures kindly provided by (a, d, f and g) Fraunhofer IST, Braunschweig [1], (b, c) IHP, Frankfurt (Oder) [2], (e) Prof. N. Hampp, University of Marburg [3]).

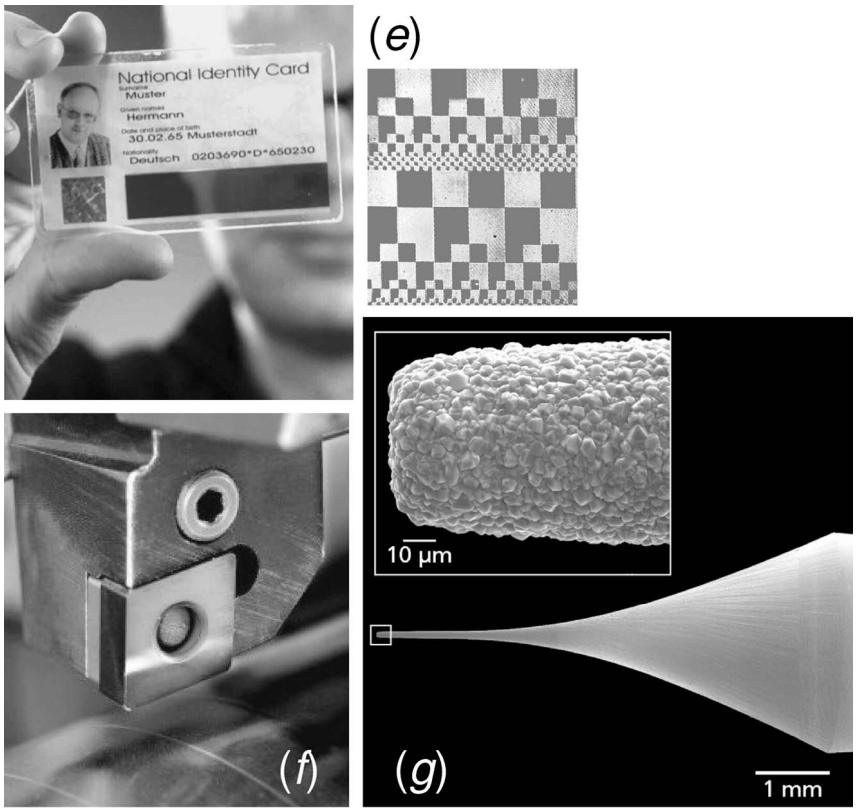

This book is intended to give overviews of the relevant x-ray scattering techniques for thin-film work and to equip scientists and engineers with the basic understanding to apply them. It has to be emphasized that for each x-ray technique presented in one of the following chapters there are authoritative and comprehensive textbooks available; these are listed at the end of each chapter and the reader is referred to them for further consultation. It seems, however, that there exists a gap between the highly developed and complex structural sciences on the one hand and the daily needs of materials scientists on the other. Many of the conclusive, effective and powerful techniques that have been developed for structural investigations appear to be not as extensively used in thin-film technology as they would deserve. It is the aim of this book to bridge this gap by introducing the concepts of x-ray techniques that appear most interesting to elucidate the close relations between structure, function and growth of thin films.

Chapter 1 introduces the basic phenomenon of x-ray diffraction by a crystalline lattice. In Chapter 2 methods for the identification of chemical phases are presented. Chapter 3 is related to the line profile analysis of diffraction peaks with respect to film microstructure. Measurement geometries characterized by a grazing incident x-ray beam are introduced in Chapter 4. The preferred orientation of crys-

tallites and residual stresses in thin films are dealt with in Chapters 5 and 6, respectively. Up to this point mostly polycrystalline films will be considered and use will be made of the kinematic theory only. Epitaxial thin films are in the focus of Chapter 7, where high-resolution x-ray diffraction is outlined and the first grounding of dynamical theory is introduced. The majority of the material presented is based on the physical phenomenon of diffraction, but some parts – as for instance the presentation of reflectometry in chapter four – are related to the more general phenomenon of x-ray scattering. This is the reason for the title of the book.

It is recommended to start reading with Chapters 1 and 2, which might be helpful even for those readers to whom the basics are already known in order to become familiar with the conventions and notation used. After this introductory training the reader may consult any other chapter presenting the method that might be expected of relevance for his or her actual work. The emphasis of the book is on x-ray scattering with laboratory setups in contrast to synchrotron radiation beam lines. However, many of the measurement concepts presented are equally realized at synchrotron facilities and may also be applied in experiments with the much higher intensity available at synchrotron sources.

Two concepts or quantities meander through the following chapters like a thread through the tows of the former British royal navy ("roter Faden" [4]). The first of these quantities is the scattering vector that is abbreviated by $\boldsymbol{Q}$ here. The scattering vector is met in almost every chapter since interatomic distances are probed by diffraction only along the direction of $\boldsymbol{Q}$. Diffraction or scattering experiments may be considered as intensity mappings under complex rotations of the sample with respect to the scattering vector. These reorientations are dealt with by the use of three reference frames $\{\boldsymbol{l}_i\}$, $\{\boldsymbol{s}_i\}$ and $\{\boldsymbol{c}_i\}$, one for each frame of the laboratory, the sample and the crystallographic unit cell. The different frames are sometimes confusing for the newcomer to the field. It is recommended that when one seems of having lost the "roten Faden" it might be taken up again by answering the question "what are the coordinates of the scattering vector $\boldsymbol{Q}$ within the respective reference frame?"

The second recurring quantity is that of the x-ray attenuation coefficient μ. In condensed matter x-rays are attenuated on a length scale of some 10 to some 100 µm. These penetration depths are accordingly often larger than the film thickness t and special methods have been developed to restrict the probing beam to the sample volume. In almost all of the forthcoming chapters we have to derive how the μt product affects the measured scattering intensities. It may even be stated that the μt product can be regarded as the central physical quantity in thin-film analysis by x-ray scattering.

The chapters end with an application section, where studies and works related to the issue of the chapter are presented. The selection of these examples and those mentioned in the main body of the text is probably highly selective and reflects the interest and working areas of the author(s). Since each chapter covers a large field of research activities it was hardly possible to overview fully the many interesting x-ray scattering investigations that have been carried out in the appropriate areas. A collection of exercises is given at the end of each chapter, by the solution of which

the reader may verify the understanding of the text. Solutions to the exercises can be found on the internet [5].

Two further issues are considered in parallel with the main text. These are related, firstly, to the instrumentation in x-ray scattering experiments and, secondly, to the structure of selected material classes. In the instrumentation boxes, the instrumentation required by the experiments described in the chapter is detailed. The structure boxes present crystallographic structures, structural parameters and selected physical properties of relevant materials. The material systems have been chosen in accordance with their relevance to illustrate the x-ray scattering technique in the chapter. The selected material systems are in order of increasing chapter number metals, semiconductors, nanocomposites, optical thin films, dielectric and superconducting materials, hard coatings and finally semiconductors for micro- and optoelectronics. Other combinations would have equally been possible.

Two remarks have to be made on notation: (a) SI units have been used throughout the text and (b) it has been endeavored to use a consistent notation throughout the text. However, this turned out a difficult task, since every chapter covers a highly developed subfield of x-ray scattering with its own nomenclature. It could thus not be completely avoided to make use of the same symbol with different meaning in different chapters. These cases will explicitly be pointed out. In case of doubt, the appropriate meaning of a symbol can be identified by consulting the symbol list.

In some cases, the names of inventors or scientific pioneers are mentioned. It should be borne in mind, however, that scientific achievements always rely on the communication among different researchers exchanging their ideas and imaginations. This statement is illustrated by the famous discussion between P.P. Ewald and M. Laue that laid the basis for the first x-ray diffraction experiments by Friedrich, Knipping and Laue [6]. Scientific progress has always been based on teamwork, even if the protagonists did not know each other personally. This fact is explicitly stated here, since we cannot be sure in every case that all the researchers that should be credited were adequately indicated when one or more of them are mentioned. Since x-ray diffraction is about 100 years old, it may be possible that future research in the history of science will reveal personal contributions of which we were not fully aware at the time of writing. The reader interested in the early history of x-ray diffraction is referred to a paper collection published for the International Union of Crystallography [7].

This book project would not have become reality without the help of some friends and colleagues. Firstly, I would like to thank Paul Fewster and Christoph Genzel for their co-authorship of Chapters 6 and 7. They both agreed on being co-authors to chapters they would be much more qualified of writing themselves and let me assume the role of the first author in order to maintain consistency with the rest of the book. Their great expertise in the respective fields helped enormously to formulate these two state-of-the-art chapters. I enjoyed the work with both of them very much. I am indebted to Daniel Chateigner, Carl Krill, Paolo Scardi, Thomas Schröder, Antonella Tagliente, Mark Vaudin, Thomas Wieder, Don Williamson, Joachim Woitok and Peter Zaumseil, who carefully red draft versions of single chapters, gave valuable recommendations and pointed me to some examples from

the work of their own and others. Moreover, I like to thank those colleagues, who permitted the reprint of figures from their publications, which are (in addition to those already mentioned) J. Almer, U. Balachandran, M. Deutsch, J. Driscoll, J. Gubicza, N. Hampp, K. Helming, Y. Iijima, D. Knoll, S. Kondruweit, L. Lutterotti, M. A. Meyer, C. Michaelsen, M. Morales, A. Navarro-Quezada, S. Peist, A. J. Perry, M. Li, R. P. Reade, Á. Révész, J. Ricote, A. Saerens, K. Saito, K. Schiffmann, S. Sun, H. Suo, T. Ungár, J. J. Wells and E. Zschech. Their work on thin film analysis will probably be very helpful to the reader by illustrating the theoretical derivations with real-world examples. Thanks are also to Jürgen Altmann and Wulff Pfeiffer for their support of this project, to the companies AMD, Bruker AXS, IfG, PANalytical, Seifert for providing pictures from their thin film or x-ray equipment products, to Cyrille Boudias and Daniel Monceau, who draw the crystallographic figures in the structure boxes by virtue of their software package CaRIne Crystallography [8] and to the Wiley-VCH Verlag, who followed all my suggestions in preparing an editing the manuscript. Most of all, I would like to thank my wife, Johanna, for her patience and continuous support of this project.

References

Monographs, conference proceedings and internet sites of general relevance

E. Prince (Ed.): *International Tables for Crystallography – Vol. C*, 3rd ed., Kluwer Academic, Dordrecht, 2004.

M. Ohring: *The Materials Science of Thin Films*, Academic Press, San Diego, 2nd ed., 2002.

International Union of Crystallography: www.iucr.ac.uk.

Proceedings of the annual Denver X-Ray Conferences (DXC) published by the International Center for Diffraction Data (ICDD)
Advances in X-ray Analysis, Vol. 48, Proceedings of the 2004 Conference, 2005, etc.

Special papers

[1] Institut für Schicht- und Oberflächentechnik, *Jahresbericht 2003*, Braunschweig, 2004.

[2] IHP, *Jahresbericht 2003*, Frankfurt (Oder), 2004, and D. Knoll, personal communication.

[3] N. Hampp, *Bakteriorhodopsin als photochromes Sicherheitspigment und biologischer Datenspeicher* (vdi, Düsseldorf, 2000).

[4] J. W. Goethe, *Wahlverwandtschaften*, Weimar, 1809.

[5] Exercise solutions: www.thinfilm-at.com.

[6] G. Hildebrandt, *75 Jahre Röntgenstrahlinterferenzen in Kristallen*, Phys. Bl. **43** (1987) 430.

[7] J. M. Bijvoet, W. G. Burgers, G. Hägg (eds.), *Early Papers on Diffraction of X-rays by Crystals*, (Published for the International Union of Crystallography by A. Oosthoek's Uitgeversmaatschappij N. V., Utrecht, 1969).

[8] C. Boudias & D. Monceau, CaRIne Crystallography 4.1, User's Guide (2004), and http://pro.wanadoo.fr/carine.crystallography/.

Symbols

Symbols consistently used throughout the book are listed in the sequence of appearance in the chapters.

Chapter 1

2θ	scattering angle
α, β, γ	angles between edges of crystallographic unit cell
δ	divergence of x-ray beam
ε_0	permittivity of a vacuum
$\phi_{\boldsymbol{h}}$	phase of diffracted plane wave
λ	x-ray wavelength
μ	linear x-ray attenuation or absorption coefficient
μ_{m}	mass attenuation coefficient
μt	product of attenuation coefficient and film thickness
σ, π	indices to denote perpendicular and parallel polarized beam components
ρ	mass density
ρ_{e}	electron density
$\tau_{1/e}$	$1/e$ penetration depth
θ	Bragg angle
$\theta_{\mathrm{B}}, 2\theta_{\mathrm{B}}$	Bragg angle and scattering angle of a Bragg reflection
$\{\boldsymbol{c_i}\}$	crystal reference frame of individual crystallites (superscript C)
$\{\boldsymbol{l_i}\}$	laboratory reference frame (superscript L)
$\{\boldsymbol{s_i}\}$	specimen reference frame (superscript S)
a, b, c	lattice parameters or cell edges of crystallographic unit cell
a_{ij}^{XY}	transformation matrices from reference frame X to Y (with $X, Y =$ C, L, S)
$\boldsymbol{b_i}$	unit cell vectors of reciprocal lattice
A	absorption factor in XRS experiment
$A(2\theta), A_{\theta/2\theta}$	absorption factor for symmetric $\theta/2\theta$ experiment
B	isotropic temperature damping factor

c	velocity of light in vacuum
C	polarization factor
$\overline{C^2}$	average polarization factor
Cu Kα	x-ray radiation from copper source (Kα line)
e	electron charge
d	interplanar spacing between crystallographic lattice planes
E	energy of radiation
$\boldsymbol{E_0}$, $\boldsymbol{E}$	electrical field vector of incoming and scattered beam
f	atomic form factor
f'	real part of anomalous scattering factor
f''	imaginary part of anomalous scattering factor
$\boldsymbol{F}$, $\boldsymbol{F^*}$	structure factor and its complex conjugate
G	geometry factor
$\boldsymbol{h}$	abbreviated form of Miller indices hkl, also used as subscript
hkl	Miller indices of Bragg reflection from (hkl) lattice planes
(hkl), {hkl}	Miller indices of crystallographic lattice plane
[hkl], ⟨hkl⟩	Miller indices of crystallographic direction
i	imaginary unit
$\Im$	interference function
I	x-ray intensity
I_0	intensity of the incident beam
I_B	maximum intensity of x-ray reflection at Bragg angle θ_B
$I_{\boldsymbol{h}}$	integrated intensity of a Bragg reflection from (hkl) lattice planes
k	geometry factor for XRS experiment
$k(2\theta)$, $k_{\theta/2\theta}$	geometry factor for symmetric $\theta/2\theta$ scan
$\boldsymbol{K_0}$	wave vector of incoming x-ray beam outside the sample
$\boldsymbol{K}$	wave vector of scattered x-ray beam outside the sample
ℓ	path length of x-ray in the sample
L	Lorentz factor
Lp	Lorentz polarization factor
m_{hkl}, $m_{\boldsymbol{h}}$	multiplicity of a Bragg reflection hkl in a powder pattern
m_0	rest mass of an electron
n	order of reflection in Bragg equation
N	number of unit cells in a crystallite
n_1, n_2, n_3	integers to denote the position of a unit cell in a crystallite
N_1, N_2, N_3	number of unit cells of a single crystallite along its orthogonal directions
N_L	Loschmidt's number
P	power of scattered x-ray beam
$\boldsymbol{Q}$	scattering vector
r	atomic distance or bond length
$\boldsymbol{r_{n_1n_2n_3}}$	distance vector from the origin of a crystallite to unit cell of number (n_1, n_2, n_3)
r_e	classical radius of the electron
R	goniometer radius

R_{FC}	radius of the focusing circle
SCF	scaling factor for x-ray intensity received by the detector
S	surface
$\boldsymbol{s_3}$	substrate normal vector
t	thickness of thin film
t'	time
T	temperature
$T_{\boldsymbol{h}}$	texture factor of $\boldsymbol{h}$th reflection
$\overline{u^2}$	mean-square oscillation amplitude due to thermal vibrations of the atom
V	irradiated sample volume
V_{uc}	unit cell volume
x_n, y_n, z_n	fractional coordinates of nth atom in the unit cell
z	thin film depth coordinate
Z	number of electrons of an atom

Chapter 2

α_1, α_2	subcomponents of α x-ray emission line
δ_a	x-ray beam divergence along the θ and 2θ axis (axial divergence)
δ_p	x-ray beam divergence in the scattering plane (equatorial divergence)
δ_{ds}	opening angle of divergence slit
δ_{rec}	opening angle of receiving slit
δ_{Sol}	opening angle of Soller slits
γ	angle between scattering vector and bond vector
ϕ	azimuth, i.e. angle of in-plane sample rotation
σ	cross-section for x-ray scattering
θ_0	centroid of Bragg reflection
$(\Delta 2\theta)_i$	instrumental shifts of centroid from Bragg peak position
a_0, a_1	coefficients in the linear expansion of unit cell edge a
b	height misalignment of sample surface
B_a, B_p	extension of x-ray foot step on the sample along axial and in-plane directions
j	numeration of layers in a multilayer stack
J	number of layers in a multilayer stack
M	atomic mass
S	subscript to denote quantities related to a substrate
T_{dep}	deposition temperature
T_{hom}	homologous temperature
T_{mel}	melting temperature
TF	subscript to denote quantities related to a thin film
w_j	weight of the jth phase in a thin-film sample
W	total weight of a thin film
x	stoichiometry coordinate of a binary compound $A_{1-x}B_x$

Chapter 3

β	integral breadth of Bragg reflection
$\beta_{2\theta}$	integral breadth on scattering angle scale
β_Q	integral breadth on the scale of momentum transfer
γ	variance of crystallite sizes in lognormal distribution function
Γ_{hkl}	ratio of the permutation invariants of fourth order polynomials of Miller indices
ε	lattice strain
$\varepsilon_{\mathrm{rms}}$	root-mean square strain
$\widetilde{\varepsilon}$	weighted average strain
λ_1, λ_2	wavelengths of subcomponents of α x-ray emission line
θ_{S}, θ_{E}	start and end value of scattering angle range
ρ_{d}	dislocation density
η	weight parameter of pV profile function indicating the Cauchy fraction
$2w$	full width at half maximum
A_n, $A(n)$	coefficients of Fourier expansion
A^{S}, A^{size}	coefficients of Fourier expansion accounting for size broadening
A^{D}, A^{dis}	Fourier expansion coefficients accounting for broadening by lattice distortions
$\boldsymbol{b}$	Burger's vector to describe geometrical structure of dislocation
$B(2\theta)$	background function in whole pattern fitting
C	Cauchy profile function
C_{hkl}	dislocation contrast factor
$\overline{C}_{hkl}$	average dislocation contrast factor
d_0	position of the centroid of a Bragg peak
D	crystallite size parameter
D_0	crystallite size median in lognormal distribution function
D_{cub}	length of a cube-shaped crystallite
D_{sph}	diameter of a spherical crystallite
$\langle D^n \rangle$	nth statistical moment of crystallite size distribution
$\langle D \rangle_{\mathrm{A}}$	area-weighted average crystallite size
$\langle D \rangle_{\mathrm{V}}$	volume-weighted average crystallite size
f	sample line profile free from instrumental effects
$\mathcal{F}(y(x))$	Fourier transform of function $y(x)$
g	instrumental line profile
$g(D)$	crystallite size distribution function
$g_{\mathrm{LN}}(D)$	logarithmic normal distribution function of crystallite size
G	Gauss profile function
G_n, $G(n)$	coefficients of Fourier expansion of standard peak
h	convolution of instrumental and sample-broadened line profile
H_n, $H(n)$	coefficients of Fourier expansion of measured sample peak
I_0	maximum peak intensity

k	parameter in Voigt profile function
K_S	Scherrer constant
K_D	scaling factor in Williamson–Hall relation and derivatives
L	correlation length
$\langle L^n \rangle$	nth statistical moment of column height distribution
m	parameter in Pearson profile function
M	dislocation configuration parameter
N	number of data points subjected to a Fourier transformation
N_3	number of unit cells in a unit cell column
pV	pseudo Voigt profile function
P	Pearson (VII) profile function
$p(L)$	column height distribution function of the sample
$P(L)$	column height distribution function of one crystallite
R	radius of spherical crystallite
R_c	core radius of dislocation
R_e	effective outer cut-off radius of dislocations
R_w	weighted R factor
R_{21}	intensity ratio of α_2 over α_1 intensity
V	Voigt profile function
$\boldsymbol{u}(\boldsymbol{r})$	displacement field or distortion field
$y(2\theta)$	model function of intensity in whole pattern fitting

Chapter 4

α, α_i	incidence angle of incident x-ray with respect to sample surface
α_f	exit angle of diffracted x-ray with respect to sample surface
α_c, θ_c	critical angle for total external reflection
α_t	angle of transmitted x-ray with respect to surface plane
β	negative imaginary part of x-ray refractive index
δ	negative deviation of real part of x-ray refractive index from unity
$\Delta(2\theta)$	shift of Bragg peak position due to refraction
k_α	geometry factor for GIXRD experiment
θ_m	maximum of Kiessig fringes in reflectivity curve
σ	root mean square roughness of film surface or interface
ρ_a	density of atoms
$\tau_{1/e}$	penetration depth
τ_{63}	penetration depth due to scattered intensity
$\overline{\tau}$	average information depth in thin film of finite thickness
$\overline{\tau}_\alpha$	average information depth in GIXRD
A_α	absorption factor for GIXRD experiment
B_+, B_-	real and negative imaginary part of α_t
E_t	amplitude of transmitted electrical field
I_R	intensity of the reflected beam
$\boldsymbol{k}$	wave vector of x-rays within the sample

$k_{z,j}$	z component of wave vector in the jth layer of a multilayer stack
$\mathfrak{L}$	Laplace transform
m	order of Kiessig fringe
$\boldsymbol{M}$	transfer matrix in XRR
n	real part of index of refraction
$\hat{n}$	complex index of refraction
$P(z)$	depth-dependent property
$\overline{P}$	property averaged over depth
$\overline{P}_{\alpha}$	depth-averaged property in GIXRD
$\boldsymbol{R}_{j,j+1}$	refraction matrix in XRR
$r_{j,j+1}$	reflection coefficient between the jth and (j+1)th layer in a multilayer stack
t_{per}	superlattice period
$\boldsymbol{T}_{j,j+1}$	translation matrix in XRR
$z(x, y)$	height function of sample surface
$\overline{z}$	average sample height

Chapter 5

$\Delta\psi$	tilt in crystallite orientation distribution, i.e. FWHM of $I_{\boldsymbol{h}}(\psi)$
$\Delta\phi$	twist in crystallite orientation distribution, i.e. FWHM of $I_{\boldsymbol{h}}(\phi)$
$\varphi_1, \Phi, \varphi_2$	Euler angles for the S $\rightarrow$ C transformation
ω	sample rotation angle on Θ axis
k_{ψ}	geometry factor for pole figure measurement
k_{ω}	geometry factor in Ω mode
$\psi_{1/2}$	FWHM of volume share of fiber fraction
ψ	tilt angle or polar angle
$\overline{\tau}_{\psi}$	average information depth in ψ scan
A_{ψ}	absorption factor in Ψ mode
A_{ω}	absorption factor in Ω mode
C_l^{μ}	coefficients in linear expansion of inverse pole figure
C_l^{mn}	coefficients in linear expansion of harmonic ODF
$C_l^{\mu\nu}$	linear coefficients in symmetry-adapted ODF expansion
$\boldsymbol{d}$	direction vector
$f(g)$	orientation distribution function
$f(\varphi_1, \Phi, \varphi_2)$	orientation distribution function
$F_l(\boldsymbol{h})$	weight factors in $I_{\boldsymbol{h}}(\psi)$ expansion
$F_e^{\nu}(\boldsymbol{h})$	pole figure coefficients of $\boldsymbol{h}$th reflection
g	orientation of a crystallite with respect to the sample reference frame
G	volume fraction of the textured phase (March model)
$I_{\boldsymbol{h}}(\psi)$	intensity distribution of Bragg reflection $\boldsymbol{h}$ for varying tilt angles
$I_{\boldsymbol{h}}(\phi)$	course of intensity of Bragg reflection $\boldsymbol{h}$ for varying azimuths
$I_{rc}(\omega)$	intensity distribution in a rocking curve scan
J	texture index

$k_l^{\mu}(\Phi, \beta)$	symmetrized spherical harmonics
$l_{\max}$	order of maximum expansion of orientation distribution function
$M(l)$	number of ODF expansion coefficients of order l
$\boldsymbol{n_h}$	normal on $\boldsymbol{h}$ lattice planes
$P_l(x)$	Legendre function
$\bar{P}_l^m(x)$	normalized associated Legendre polynomial
$P_l^{mn}(x)$	generalized associated Legendre polynomial
r	ratio of t_i over t_f (March model)
$R(\beta, \Phi)$	inverse pole figure
t_i, t_f	initial and final thickness of rolled metal sheet
$T_l^{mn}(x)$	generalized harmonics
$T_l^{\mu\nu}$	symmetry-adopted generalized harmonics
$V_f(\psi)$	volume share of fiber texture between tilt angle 0 and ψ

Chapter 6

α, β	incidence and exit angle of x-rays
α	coefficient of thermal expansion
$\Delta\alpha$	difference of coefficients of thermal expansion between layer and substrate
ε_{ij}	strain tensor
ε_{ij}^{L}, ε_{ij}^{S}	strain tensor in the laboratory and specimen reference frame
$k_{\alpha\beta}$	geometry factor for general incidence and exit angle
k_η	geometry factor in the scattering vector technique
ν	Poisson ratio
η	angle of rotation around the scattering vector
H	rotation axis parallel to the scattering vector
σ_{ij}	stress tensor
$\sigma_{\parallel}$	residual stress in the film plane
$\sigma_{\parallel}(z)$	stress gradient for in-plane residual stress
σ_{ij}^{L}, σ_{ij}^{S}	stress tensor in the laboratory and specimen reference frame
σ^{I}, σ^{II}, σ^{III}	residual stresses of first, second and third kind
ψ^*	stress-free tilt angle
$\tau_{\psi\eta}(\theta)$	penetration depth in scattering vector mode
$\tau_{1/e}(\alpha)$	$1/e$ penetration depth for incidence angle α under inclusion of absorption
$A_{\alpha\beta}$	absorption factor for general incidence and exit angle
A_η	absorption factor in the scattering vector mode
c_{ijkl}, C_{ijkl}	elastic stiffness tensor of single crystal and polycrystalline aggregate
d_0	stress-free interplanar spacing
$d_\perp$	interplanar spacing of surface-parallel lattice planes
$d_{\phi\psi}$	interplanar spacing as determined for azimuth ϕ and tilt angle ψ
$d(\psi)$, d_ψ	distribution of d values as a function of tilt angle
E	Young's modulus

F_{ij}	anisotropic stress factors
R	bending radius of layer–substrate composite due to residual stress
s_{ijkl}, S_{ijkl}	elastic compliances tensor of single crystal and polycrystalline aggregate
s_0	anisotropy constant
s_1, $1/2s_2$	diffraction elastic constants DEC
t_{ijkl}	elastic polarizability tensor

Chapter 7

Δ	standard deviation in orientation distribution of mosaic blocks and crystallites
Δ_ϕ	standard deviation of in-plane orientation distribution (twist)
Δ_ψ	standard deviation of out-of-plane orientation distribution (tilt)
$\Delta\lambda$	bandwidth of x-ray radiation
γ	asymmetry parameter
γ_o	sin of the inclination angle to the film surface
γ_h	sin of the angle of emergence to the film surface
κ	elastic stiffness-dependent parameter
$\widetilde{\mu}$	extinction coefficient
$\nu 0_L$, $\nu 1_L$	linear expansion coefficient of Poisson's ratio
η	deviation parameter
χ	crystal polarizability
τ_{ex}	extinction length
Δa	absolute lattice mismatch
$\Delta d_\perp$	lattice spacing difference between substrate and layer peak in symmetric scan
a_L, a_S	unit cell edges of cubic layer (L) and substrate (S) material
$a_{\|\|}$, $a_\perp$	in-plane and out-of-plane unit cell edges of tetragonally distorted layers
$a^0{}_L$, $a^1{}_L$	linear coefficients of unit cell edge in Vegard's rule
$f(p)$	primary extinction correction
$\boldsymbol{D}$	dielectric displacement vector
$\boldsymbol{k}_0$	wave vector of primary x-ray beam inside the sample
$\boldsymbol{k}_h$	wave vector of diffracted x-ray beam inside the sample
m	relative lattice mismatch
$\boldsymbol{q}$	scattering vector inside the sample
Q_x, Q_z	in-plane and out-of-plane component of scattering vector
R	relaxation parameter
t_c	critical thickness
W	tilt distribution function of mosaic blocks
x	composition variable
X_0, X_h	excitation errors (Anregungsfehler)

1
Principles of X-ray Diffraction

Diffraction effects are observed when electromagnetic radiation impinges on periodic structures with geometrical variations on the length scale of the wavelength of the radiation. The interatomic distances in crystals and molecules amount to 0.15–0.4 nm which correspond in the electromagnetic spectrum with the wavelength of x-rays having photon energies between 3 and 8 keV. Accordingly, phenomena like constructive and destructive interference should become observable when crystalline and molecular structures are exposed to x-rays.

In the following sections, firstly, the geometrical constraints that have to be obeyed for x-ray interference to be observed are introduced. Secondly, the results are exemplified by introducing the $\theta/2\theta$ scan, which is a major x-ray scattering technique in thin-film analysis. Thirdly, the $\theta/2\theta$ diffraction pattern is used to outline the factors that determine the intensity of x-ray reflections. We will thereby rely on numerous analogies to classical optics and frequently use will be made of the fact that the scattering of radiation has to proceed coherently, i.e. the phase information has to be sustained for an interference to be observed.

In addition, the three coordinate systems as related to the crystal $\{\boldsymbol{c}_i\}$, to the sample or specimen $\{\boldsymbol{s}_i\}$ and to the laboratory $\{\boldsymbol{l}_i\}$ that have to be considered in diffraction are introduced. Two instrumental sections (Instrumental Boxes 1 and 2) related to the $\theta/2\theta$ diffractometer and the generation of x-rays by x-ray tubes supplement the chapter. One-elemental metals and thin films composed of them will serve as the material systems for which the derived principles are demonstrated. A brief presentation of one-elemental structures is given in Structure Box 1.

1.1
The Basic Phenomenon

Before the geometrical constraints for x-ray interference are derived the interactions between x-rays and matter have to be considered. There are three different types of interaction in the relevant energy range. In the first, electrons may be liberated from their bound atomic states in the process of photoionization. Since energy and momentum are transferred from the incoming radiation to the excited electron, photoionization falls into the group of inelastic scattering processes. In

addition, there exists a second kind of inelastic scattering that the incoming x-ray beams may undergo, which is termed Compton scattering. Also in this process energy is transferred to an electron, which proceeds, however, without releasing the electron from the atom. Finally, x-rays may be scattered elastically by electrons, which is named Thomson scattering. In this latter process the electron oscillates like a Hertz dipole at the frequency of the incoming beam and becomes a source of dipole radiation. The wavelength λ of x-rays is conserved for Thomson scattering in contrast to the two inelastic scattering processes mentioned above. It is the Thomson component in the scattering of x-rays that is made use of in structural investigations by x-ray diffraction.

Figure 1.1 illustrates the process of elastic scattering for a single free electron of charge e, mass m and at position $\boldsymbol{R}_0$. The incoming beam is accounted for by a plane wave $\boldsymbol{E}_0\exp(-\mathrm{i}\boldsymbol{K}_0\boldsymbol{R}_0)$, where $\boldsymbol{E}_0$ is the electrical field vector and $\boldsymbol{K}_0$ the wave vector. The dependence of the field on time will be neglected throughout. The wave vectors $\boldsymbol{K}_0$ and $\boldsymbol{K}$ describe the direction of the incoming and exiting beam and both are of magnitude $2\pi/\lambda$. They play an important role in the geometry of the scattering process and the plane defined by them is denoted as the scattering plane. The angle between $\boldsymbol{K}$ and the prolonged direction of $\boldsymbol{K}_0$ is the scattering angle that will be abbreviated by 2θ as is general use in x-ray diffraction. We may also define it by the two wave vectors according to

$$2\theta = \arccos\frac{\langle \boldsymbol{K}, \boldsymbol{K}_0 \rangle}{KK_0} \tag{1.1}$$

The formula is explicitly given here, because the definition of angles by two adjoining vectors will be made use of frequently.

The oscillating charge e will emit radiation of the same wavelength λ as the primary beam. In fact, a phase shift of 180° occurs with the scattering, but since this shift equally arises for every scattered wave it has no effect on the interference pattern in which we are interested and will be neglected. If the amplitude of the scattered wave $\boldsymbol{E}(\boldsymbol{R})$ is considered at a distance $\boldsymbol{R}$ we may write according to Hertz and Thomson

$$\boldsymbol{E}(\boldsymbol{R}) = \boldsymbol{E}_0 \frac{1}{4\pi\varepsilon_0 R}\frac{e^2}{mc^2}\sin\angle(\boldsymbol{E}_0, \boldsymbol{R})\exp(-i\boldsymbol{K}\boldsymbol{R}) \tag{1.2}$$

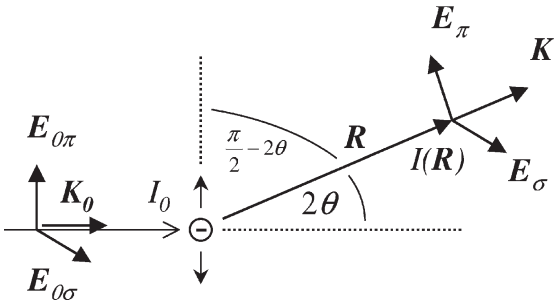

Figure 1.1 Scattering of x-rays by a single electron.

where ε_0 and c are the vacuum permittivity and velocity of light. The field vector $\boldsymbol{E}$ and wave vector $\boldsymbol{K}$ are oriented perpendicular to each other as is usual for electromagnetic waves. The sin term is of significance when the state of polarization is considered for which two extreme cases may arise. In one case, the exciting field $\boldsymbol{E}_0$ is confined to the scattering plane and in the second case it is normally oriented. In classical optics these two cases are named π polarization and σ polarization. The field vectors in both cases will be denoted by $\boldsymbol{E}_\pi$ and $\boldsymbol{E}_\sigma$. The angle between $\boldsymbol{E}_\sigma$ and $\boldsymbol{R}$ is always 90° and the sin term will equal unity. For the case of π polarization, however, it may be expressed by virtue of the scattering angle according to $\sin\angle(\boldsymbol{E}_0, \boldsymbol{R}) = |\cos 2\theta|$. If the character C abbreviates the sin term it may be written

$$C = \begin{cases} 1 & \sigma\text{-polarization} \\ |\cos 2\theta| & \pi\text{-polarization} \end{cases} \tag{1.3}$$

Since the intensity is obtained from the sum of the square of both field vectors the expression

$$\left(\frac{1}{4\pi\varepsilon_0 R}\right)^2 \left(\frac{e^2}{mc^2}\right)^2 \left(E_\sigma^2 + E_\pi^2 \cos^2 2\theta\right) \tag{1.4}$$

is obtained. In a nonpolarized beam both polarization states will have the same probability of occurring,

$$\overline{E_\sigma^2} = \overline{E_\pi^2} = I_0 / 2$$

and it is finally arrived at the intensity of the scattered beam at distance R

$$I(\boldsymbol{R}) = I_0 \frac{r_e^2}{R^2} \frac{1 + \cos^2 2\theta}{2} \tag{1.5}$$

Here, use has been made of the notion of the classical radius of the electron, $r_e = e^2/(4\pi\varepsilon_0 mc^2)$, that amounts to 2.82×10^{-15} m. The intensity of the scattering is seen to scale with the inverse of R^2 as might have been expected. It can also be seen that $I(\boldsymbol{R})$ scales with the ratio of squares of r_e over R. Since distances R of the order of 10^{-1} m are realized in typical laboratory setups the probability of observing the scattering by a single electron tends to zero. The situation substantially improves if the number of scattering objects is of the same order of magnitude as Loschmidt's number N_L – as usually is the case in experiments.

It also becomes evident from this equation as to why the scattering from atomic nuclei has not been considered in the derivation. In fact, the equation would also hold for the scattering from atomic nuclei, but it can be seen from Eq. (1.4) that the nuclei component will only yield a less than 10^{-6} smaller intensity compared to an electron. The difference is simply due to the mass difference, which is at least larger by a factor of 1836 for any atomic species. The scattering of x-rays by nuclei may, therefore, confidently be neglected. From the viewpoint of x-ray scattering an atom can thus be modeled by the number of Z electrons, which it contains according to its rank in the periodic table. In terms of the Thompson scattering model Zr_e may be written in Eq. (1.3) instead of r_e in order to describe the scattering from an atom,

since the primary beam is then equally scattered by all electrons. In addition, it will be assumed temporarily that all electrons are confined to the origin of the atom. The consequences that follow from a refinement of the model by assuming a spatially extended charge distribution will be postponed to a later section. Hence, we have a first quantitative description for the x-ray elastic scattering from an atom.

In the next step consideration is given to what the scattering will look like if it occurs for a whole group of atoms that are arranged in a periodically ordered array like a crystal lattice. Figure 1.2 visualizes such an experiment where the crystal is irradiated with monochromatic x-rays of wavelength λ. In the special case considered here, each atom is surrounded by six neighbor atoms at distance a and the angle between two atomic bonds is always 90° or multiples of it. Atomic positions can then be described by the lattice vector $\boldsymbol{r}_{n_1n_2n_3} = n_1a\boldsymbol{c}_1 + n_2a\boldsymbol{c}_2 + n_3a\boldsymbol{c}_3$ with $\boldsymbol{c}_1$, $\boldsymbol{c}_2$ and $\boldsymbol{c}_3$ being the unit vectors of the three orthogonal directions in space. The $\boldsymbol{c}_i$ axes are the unit vectors of the crystal coordinate system $\{\boldsymbol{c}_i\}$, which is assigned to the crystal. For some properties of the crystal this coordinate system will turn out to be extremely useful and the notion will be used throughout the book. The shape of the crystal is assumed to be that of a parallelepiped as is accounted for by the inequalities $0 \leq n_i = N_i - 1$ for $i = 1, 2, 3$. Each node of adjacent cubes is thus occupied by an atom. Such a structure is called simple cubic in crystallography. Only a single element crystallizes in this structure, which is polonium exhibiting an interatomic distance of $a = 0.3359$ nm. Although this metal has only very few applications, the case shall be considered here in detail, because of its clarity and simplicity.

It will now be calculated at which points in space interferences of x-rays might be observed that arise due to the scattering at the crystal lattice. The task is to quantify the strength of the scattered fields at a point $\boldsymbol{R}$ when elastic scattering occurs according to Eq. (1.5) at all atoms. The reference point of $\boldsymbol{R}$ is chosen such that it starts at the origin of the crystal lattice $\boldsymbol{r}_{000}$. This means that we relate the phase difference in the summation of all scattered fields to their phase at $\boldsymbol{r}_{000}$. This choice is arbitrary and any other lattice point might have been equally selected.

The wave vector of the primary beam $\boldsymbol{K}_0$ is assumed to be parallel to the [100] direction of the crystal. The scattering plane defined by $\boldsymbol{K}_0$ and $\boldsymbol{K}$ may coincide with one of the (010) planes. The wavefronts of the incoming plane waves which are the planes of constant phase are then oriented parallel to (100) planes. An atom on the position $\boldsymbol{r}_{n_1n_2n_3}$ would then cause a scattering intensity to be measured at $\boldsymbol{R}$ of the strength

$$E_0 \exp(-i\boldsymbol{K}_0\boldsymbol{r}_{n_1n_2n_3}) \frac{Zr_e}{\left|\boldsymbol{R} - \boldsymbol{r}_{n_1n_2n_3}\right|} \sin\angle(\boldsymbol{E}_0, \boldsymbol{R} - \boldsymbol{r}_{n_1n_2n_3}) \exp(-i\boldsymbol{K}(\boldsymbol{R} - \boldsymbol{r}_{n_1n_2n_3})) \qquad (1.6)$$

This expression differs from Eq. (1.2) essentially by the fact that $\boldsymbol{R} - \boldsymbol{r}_{n_1n_2n_3}$ occurs instead of $\boldsymbol{R}$, and for $n_1 = n_2 = n_3 = 0$ it becomes equal to Eq. (1.2). The solution of our task would simply consist in a summation over all fields scattered by the number of $N_1 \times N_2 \times N_3$ atoms comprising the crystal. However, the physics of the solution will become more transparent when an important approximation is made.

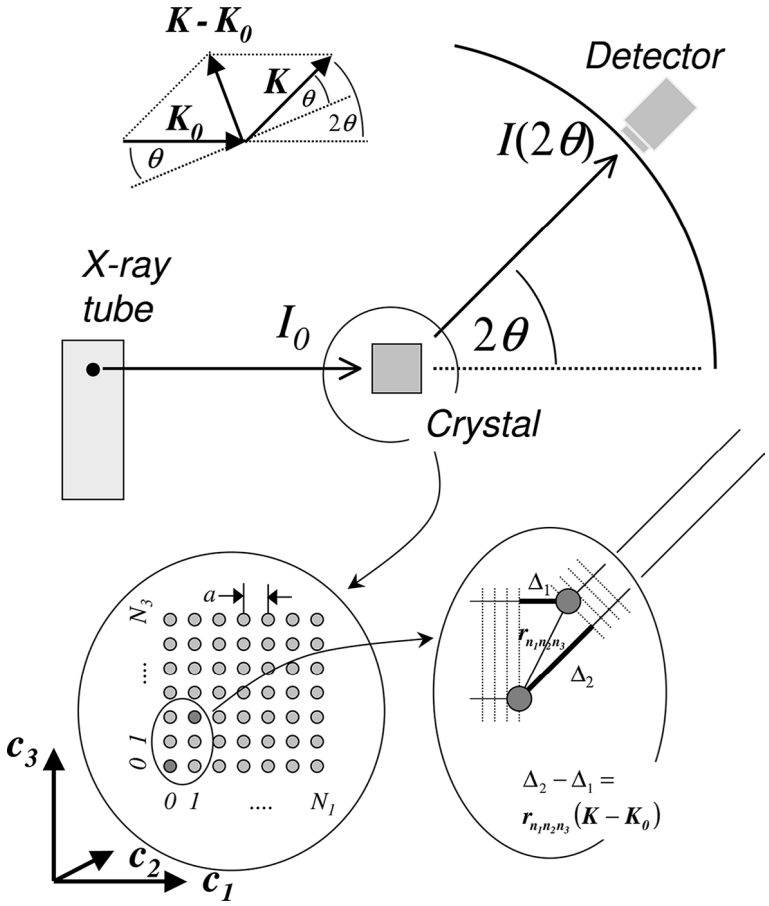

Figure 1.2 Scattering of x-rays by a crystallite of simple cubic structure.

It will be assumed that the interatomic distances r_{n1n2n3} (~10^{-10} m) are much smaller than the distances to the point of the intensity measurement $R - r_{n1n2n3}$ (~10^{-1} m). The denominator in Eq. (1.6) and in the sin term $\boldsymbol{R} - \boldsymbol{r}_{n_1n_2n_3}$ may then be replaced by $\boldsymbol{R}$ without introducing a large error. This substitution, however, is not allowed in the exponent of the last factor, since the interatomic distances are of the order of the wavelength and every phase shift according $\boldsymbol{K}\boldsymbol{r}_{n_1n_2n_3} = 2\pi r_{n1n2n3}/\lambda$ has to be fully taken into account in the summation procedure. If these rules are applied the sin term may be replaced by the polarization factor C and the sum over all scattered fields reads

$$\boldsymbol{E}_0 \frac{Zr_e}{R} C \exp\left(-i\boldsymbol{K}\boldsymbol{R}\right) \sum_{n_1n_2n_3} \exp\left(-i(\boldsymbol{K} - \boldsymbol{K}_0)\boldsymbol{r}_{n_1n_2n_3}\right) \tag{1.7}$$

All terms independent of the lattice vector $\boldsymbol{r}_{n_1 n_2 n_3}$ could be placed in front of the summation symbol. The approximation of which we have made use of is named Fraunhofer diffraction, which is always a useful approach when the distances between scattering objects are much smaller than the distance to the measurement point. In contrast to this approach stands the so-called Fresnel diffraction, for which interference phenomena are investigated very close to the scattering objects. The case of Fresnel diffraction will not be of interest here.

We have achieved a significant progress in solving our task by applying the Fraunhofer approximation and arriving at Eq. (1.7). It can be seen that the scattered field scales with two factors, where the first has the appearance of a spherical wave while the second is a sum over exponentials of vector products of wave vectors and lattice vectors. In order to improve our understanding of the summation over so many scattering centers the geometry is shown in the lower part of Fig. 1.2. A closer look at the figure reveals that the phase shift for two waves (a) scattered at $\boldsymbol{r}_{000}$ and (b) scattered at $\boldsymbol{r}_{n_1 n_2 n_3}$ comprises two components due to $\boldsymbol{K}_0 \boldsymbol{r}_{n_1 n_2 n_3}$ and to $\boldsymbol{K}\boldsymbol{r}_{n_1 n_2 n_3}$. The strength of the total scattered field of Eq. (1.7) thus sensitively depends on the spatial orientation of the wave vectors $\boldsymbol{K}_0$ and $\boldsymbol{K}$ with respect to the crystal reference frame $\{\boldsymbol{c}_i\}$.

Because a single phase shift depends on the vector product between the lattice vector and the wave vector difference $\boldsymbol{K} - \boldsymbol{K}_0$ the latter quantity is recognized as a physical quantity of its own significance and is named the scattering vector

$$\boldsymbol{Q} = \boldsymbol{K} - \boldsymbol{K}_0 \tag{1.8}$$

The scattering vector has the dimensionality of an inverse length, while its direction points along the bisection of incoming and scattered beam. The geometry is demonstrated in Fig. 1.3 and a closer inspection tells that the relation $|\boldsymbol{Q}| = 4\pi\sin\theta/\lambda$ holds for the scattering vector magnitude. This relation will be made use of extensively throughout the book and the reader should be fully aware of its derivation from Fig. 1.3. It should be realized that $|\boldsymbol{Q}|$ depends on both (a) the geometry of the scattering process via θ and (b) the wavelength λ of the probing x-ray beam. The physical meaning of $\boldsymbol{Q}$ in a mechanical analogy is that of a momentum transfer. By analogy with the kinetic theory of gases the x-ray photon

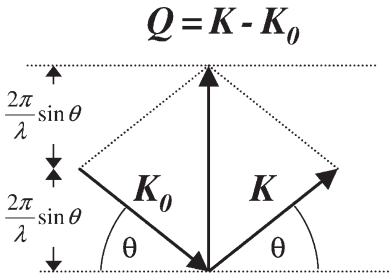

Figure 1.3 Geometry of scattering vector construction.